UC Irvine
UC Irvine Previously Published Works

Title

Human brain imaging of nicotinic acetylcholine α4β2* receptors using [^{18}F]Nifene: Selectivity, functional activity, toxicity, aging effects, gender effects, and extrathalamic pathways.

Permalink

https://escholarship.org/uc/item/3hg1g6rh

Journal

The Journal of comparative neurology, 526(1)

ISSN

0021-9967

Authors

Mukherjee, Jogeshwar
Lao, Patrick J
Betthauser, Tobey J
et al.

Publication Date

2018

DOI

10.1002/cne.24320

Peer reviewed

Human brain imaging of nicotinic acetylcholine α4β2* receptors using [18F]Nifene: Selectivity, functional activity, toxicity, aging effects, gender effects, and extrathalamic pathways

Jogeshwar Mukherjee[1], Patrick J. Lao[2], Tobey J. Betthauser[2], Gurleen K. Samra[1], Min-Liang Pan[1], Ishani H. Patel[1], Christopher Liang, Raju Metherate[3], and Bradley T. Christian[2]

[1]Preclinical Imaging, Department of Radiological Sciences, University of California, Irvine, California

[2]Department of Medical Physics and Waisman Center, University of Wisconsin, Madison, Wisconsin

[3]Department of Neurobiology and Behavior, University of California, Irvine, California

Abstract

Nicotinic acetylcholinergic receptors (nAChR's) have been implicated in several brain disorders, including addiction, Parkinson's disease, Alzheimer's disease and schizophrenia. Here we report in vitro selectivity and functional properties, toxicity in rats, in vivo evaluation in humans, and comparison across species of [18F]Nifene, a fast acting PET imaging agent for α4β2* nAChRs. Nifene had subnanomolar affinities for hα2β2 (0.34 nM), hα3β2 (0.80 nM) and hα4β2 (0.83 nM) nAChR but weaker (27–219 nM) for hβ4 nAChR subtypes and 169 nM for hα7 nAChR. In functional assays, Nifene (100 μM) exhibited 14% agonist and >50% antagonist characteristics. In 14-day acute toxicity in rats, the maximum tolerated dose (MTD) and the no observed adverse effect level (NOAEL) were estimated to exceed 40 μg/kg/day (278 μg/m²/day). In human PET studies, [18F] Nifene (185 MBq; <0.10 μg) was well tolerated with no adverse effects. Distribution volume ratios (DVR) of [18F]Nifene in white matter thalamic radiations were ~1.6 (anterior) and ~1.5 (superior longitudinal fasciculus). Habenula known to contain α3β2 nAChR exhibited low levels of [18F] Nifene binding while the red nucleus with α2β2 nAChR had DVR ~1.6–1.7. Females had higher [18F]Nifene binding in all brain regions, with thalamus showing >15% than males. No significant aging effect was observed in [18F]Nifene binding over 5 decades. In all species (mice, rats, monkeys, and humans) thalamus showed highest [18F]Nifene binding with reference region ratios >2 compared to extrathalamic regions. Our findings suggest that [18F]Nifene PET may be used to study α4β2* nAChRs in various CNS disorders and for translational research.

Correspondence: Jogesh Mukherjee, Ph.D., B138 Medical Sciences, Department of Radiological Sciences, University of California – Irvine, Irvine, CA 92697-5000, j.mukherjee@uci.edu.

ORCID

Jogeshwar Mukherjee http://orcid.org/0000-0003-1009-877X

Keywords

cortical pathway; receptor selectivity; RRID:SCR_005279; RRID:SCR_007416; RRID:SCR_014214; thalamus; translational research; white matter tracts

1 | INTRODUCTION

Nicotinic acetylcholinergic receptors (nAChR's) have been implicated in several brain disorders, including psychiatric disorders (Kutlu, Parikh, & Gould, 2015), addiction (D'Souza, 2016), Parkinson's disease (Quik, Bordia, Zhang, & Perez 2015), Alzheimer's disease (Lombardo & Maskos, 2015) and schizophrenia (Parikh, Kutlu, & Gould 2016). The β2*subtypes, which comprises of α4β2, α3β2, and α2β2 (collectively referred as α4β2* in this article since α4β2 is in higher concentrations in the brain) for which nicotine has a high affinity, have been investigated using imaging methods (e.g., Horti, Kuwabara, Holt, Dannals, & Wong 2013; Nees 2015). Nicotine, labeled with carbon-11 (Figure 1a), has been well-studied and valuable human brain kinetics information has been obtained (Garg, Lokitz, Nazih, & Garg 2017; Nyback, Halldin, Ahlin, Curvall, & Eriksson 1994; Zuo et al., 2017). Nevertheless, quantification of receptor binding was difficult (Nyback et al., 1994). Majority of human PET studies have been obtained using [^{18}F]2-FA85380 (e.g., Sultzer et al., 2017). However, subject compliance due to the long scan times (up to 6 hr) of the radioligand has been a concern for human studies (Brody et al., 2009). Therefore, newer PET imaging agents are now being suggested for studies of the elderly and challenged subjects (Declercq, Vandenberghe, Von Laere, Verbruggen, & Bormans 2016). New PET radioligands such as [^{18}F]flubatine, [^{18}F]AZAN, and [^{18}F] XTRA with faster brain kinetics for α4β2* receptors have been evaluated in humans (e.g., Sabri et al., 2015; Kuwabara et al., 2016).

Technical capability of using a radioligand with faster in vivo kinetics for imaging α4β2* receptors has been developed in our laboratory. Our tracer design included the pyridinylether backbone which led to the successful development of novel radiotracer [^{18}F]Nifene (Figure 1b). A major advantage of [^{18}F]Nifene is the significantly shorter scan time to provide quantitative PET data (40 min, Lao et al., 2017). A shorter scan time is important for several reasons: (1) Patient comfort, especially when the scans are to be carried out on the elderly and ailing population and thus improve subject compliance; (2) Motion artifacts, which often accompany scans and are critical with higher resolution scanners; and (3) Scanner time, due to increased volume of PET studies, scanner time is limited. Compared to existing agents (Kuwabara et al., 2016), [^{18}F]Nifene has shown to be superior in terms of imaging times in all species, providing reasonable target-to-nontarget ratios and providing the ability to visualize extrathalamic receptors (Lao et al., 2017).

Ligand binding site of the α4β2* nAChR across the various species is highly conserved (Albuquerque, Pereira, Alkondon, & Rogers, 2009), suggesting a high degree of similarity in receptor-ligand interaction. However, brain distribution of the α4β2* nAChR has been known to vary across species as shown by the mRNA localization of α2, α3, α4, and β2 subunits in rat (Wada et al., 1989) and monkey brain (Han et al., 2000). Our previously

reported biological properties of [^{18}F] Nifene in rodents (Kant et al., 2011; Bieszczad et al., 2012), monkeys (Pichika et al., 2006; Hillmer et al., 2011, 2013), and humans (Lao et al., 2017) suggest some regional variations of binding of [^{18}F]Nifene in the brain across the different species. Additional constraints in the different species occur due to resolution of scanners for a mouse (~25 g), rat (~250 g), monkey (~10,000 g), and human (~70,000g) as previously discussed for serotonin 5-HT$_{1A}$ receptor imaging agent [18F]Mefway (Mukherjee et al., 2016).

To further ascertain the usefulness of [^{18}F]Nifene imaging of α4β2* nAChR in humans, we report the following in this article: (1) Detailed in vitro receptor selectivity of Nifene in human cloned receptors; (2) Functional properties of Nifene compared to nicotine; (3) Toxicology study of Nifene in rats; (4) [^{18}F]Nifene binding in the human brain regions for receptor subtypes; (5) Evaluation of [^{18}F]Nifene binding in white matter thalamocortical radiations in human brain regions. These have been studied by high-field MRI (Cho et al., 2015), and shown to be responsive to nicotine using diffusion tensor imaging (DTI) (Kochunov et al., 2013); (6) Aging effects on [^{18}F]Nifene binding in the human brain; (7) Gender effects on [^{18}F]Nifene binding in the human brain; and (8) Species comparisons of [^{18}F]Nifene binding in the brain.

2 | METHODS

2.1 | General Methods

Nifene and 2-nitronifene precursor were prepared in house using reported methods (>95% purity, Pichika et al., 2006) or purchased from ABX, Germany. Other chemicals and solvents were of analytical or HPLC grade from Sigma-Aldrich (St. Louis, MO) and Fisher Scientific (Hanover Park, IL). [^{18}F]Fluoride ion was produced in the Scandotronix MC-17 cyclotron or a Siemen's RDS 112 cyclotron or a GE PETTrace cyclotron using oxygen-18 enriched water ([^{18}O] to [^{18}F] using p, n reaction). [^{18}F]Fluoride radioactivity was counted in a Capintec CRC-15R dose calibrator. All rodent studies were approved by the Institutional Animal Care and Use Committee (IACUC) of University of California, Irvine. Monkey studies were approved by IACUC of Wright State University, Dayton, Ohio and by the IACUC of University of Wisconsin, Madison. Human studies were carried out under an approved Food and Drug Administration Investigational New Drug application for [^{18}F]Nifene and with Institutional Review Board approval from University of Wisconsin, Madison.

2.2 | Radiopharmaceutical

The radiosynthesis of [^{18}F]Nifene was performed using nucleophilic displacement of the nitro group in *N*-BOC-nitronifene precursor by [^{18}F]fluoride in an automated synthesizer followed by deprotection using previously described procedures for the various species (Pichika et al., 2006; Hillmer et al., 2011). The final formulation of [^{18}F]Nifene was carried out using sterile saline (0.9% NaCl injection, United States Pharmacopeia) followed by sterile filtration through a membrane filter (0.22 μm) into a sterile dose vial for use in the PET studies. Radiochemical purity of [^{18}F]Nifene was >98% and chemical purity was found to be >95% with a measured molar activity >70 GBq/μmol (>2 Ci/μmol) at the end of synthesis.

2.3 | Receptor Binding Assays

Binding affinity measurements of Nifene in human cloned receptors were carried out by the National Institutes of Mental Health (NIMH) psychoactive drug screening program (PDSP). Binding affinity measurements of Nifene and nicotine as reference compound on human cloned receptors were carried out using [^{3}H]epibatidine and [^{125}I]α-bungara-toxin. Data represents mean % inhibition (N=4 determinations) for compound tested at receptor subtypes. Significant inhibition was considered >50% at a 10 μM Nifene concentration at the different receptor sites. In vitro affinity studies of Nifene to α4β2* nAChR in rat brain homogenates (Pichika et al., 2006) and rat brain slices were previously reported using [^{3}H]cytisine (Easwaramoorthy et al., 2007).

2.4 | Functional Assays

Functional assays of Nifene used [^{86}Rb$^+$]rubidium efflux from cells expressing α4β2* cells. Agonist and antagonist effects were determined by measuring stimulated [^{86}Rb$^+$]rubidium efflux from YXα3β4H1 or YXα4β2H1 cells that stably express functional human α3β4 and human α4β2 nAChR subtypes, respectively. The agonist effect of Nifene was determined by measuring stimulated [^{86}Rb$^+$] rubidium efflux in presence of 100 μM Nifene. Net stimulated [^{86}Rb$^+$] efflux by 100 μM nicotine was considered as 100%. Significant agonist activity was defined as stimulating a net increase of [^{86}Rb$^+$]rubidium efflux that is equal or greater than 25% of [^{86}Rb$^+$]rubidium efflux stimulated by 100 μM nicotine. Data represent mean % of stimulation of four determinations.

The antagonist effect was determined by measuring inhibition of 100 μM nicotine-stimulated [^{86}Rb$^+$]rubidium efflux by 3 concentrations of Nifene (at 1, 10 and 100 μM for a compound). Net stimulated [^{86}Rb$^+$]rubidium efflux by 100 μM nicotine as 0% inhibition. Significant antagonist activity was defined as inhibiting [^{86}Rb$^+$]rubidium efflux stimulated by 100 μM nicotine in a concentration-dependent manner, and inhibiting more than 25% of the nicotine-stimulated [^{86}Rb$^+$]rubidium efflux at median concentration tested. Data represent mean % of inhibition of four determinations.

2.5 | Toxicity Studies

The objectives of this study were to determine the safety profile and estimate the Maximum Tolerated Dose (MTD) and No Observable Adverse Effect Level (NOAEL) of Nifene. Adult male (180–250 g) and female (150–220g) Sprague-Dawley rats (Charles River, Wilmington, MA RRID:RGD_737891) were administered three intravenous doses of 1.6, 20 and 40 μg/kg/day (11.1, 139 or 278 μg/m^2/day) on Days 1, 3, and 5 followed by 15 days recovery period. This expanded acute toxicity study of Nifene was carried out by Stanford Research Laboratories (SRI International, Menlo Park, CA). Clinical observations included altered clinical signs including motor and behavioral activities, changes in body weight, food consumption, ophthalmologic examination, clinical pathology on blood samples, hematology parameters, serum chemistry, and urinalysis. After euthanasia, histopathologic examination of organ tissues were processed and evaluated.

2.6 | PET studies

Mouse (BALB\c 25–30 g) [18F]Nifene PET/CT brain scans (Constantinescu, Garcia, Mirbolooki, Pan, & Mukherjee, 2013) and rat (Sprague-Dawley 250–400 g) brain scans (Kant et al., 2011) were acquired on the preclinical Inveon PET/CT scanner (Siemens Medical Solutions, Knoxville, TN) with a resolution of 1.46 mm (FWHM) (Constantinescu & Mukherjee, 2009). Mice and rats were anesthetized with 4% isoflurane and positioned in the PET/CT scanner and maintained on isoflurane (2% for mice and 2.5% for rats) for the duration of the PET scan. Dynamic PET data was acquired with a bolus injection of [18F]Nifene (approximately 9.25 MBq (0.25 mCi) for mice and 24 MBq (0.65 mCi for rats) for up to 120 min. PET data acquisition was followed by a CT scan for attenuation correction and anatomical delineation of mouse and rat PET images. Images were analyzed using ASIPro VM (Concorde Microsystems Inc., Knoxville, TN) and Pixelwise Modeling Software (PMOD Technologies Ltd, Zurich, Switzerland).

[18F]Nifene PET studies in rhesus monkey (*Macaca mulatta* 8–10 kg) were carried out either on Siemens ECAT EXACT HR+ PET scanner with in-plane FWHM of 4.6 mm (Pichika et al., 2006) or in the Concorde P4 MicroPET scanner with in-plane spatial resolution of 1.8 mm (Hillmer et al., 2011). Anesthesia was either ketamine (10 mg/kg, IM) and xylazine (0.5 mg/kg, IM) or ketamine (10 mg/kg, IM) and atropine sulfate (0.27 mg, IM) and isoflurane (1–2%) for the duration of the PET scan. After a bolus injection of approximately 48–111 MBq (1.3–3 mCi) of 18F-Nifene, PET data were acquired for at least 120 min. Areas showing maximal radioligand binding in the thalamus, cortex and other brain regions were delineated in the images. A rhesus brain MRI image template was used to coregister the PET images (Hillmer et al., 2011).

Human subjects, 21–69 years old and in good health (4 males, 4 females) provided written informed consent. Subjects on any psycho-tropic medication that interacts with α4β2* nAChRs, smokers or had a positive pregnancy test were excluded. Studies were conducted under an FDA-approved investigational new drug application for [18F]Nifene, and with the approval of the Institutional Review Board at the University of Wisconsin-Madison. More details of the study were recently reported (Lao et al., 2017). Human [18F]Nifene PET data were acquired on a Siemens ECAT EXACT HR+ PET scanner using 3-D mode in-plane FWHM of 4.6 mm. Dynamic PET data acquisition was initiated with a bolus injection of approximately 185 MBq (5 mCi) [18F]Nifene, and data were acquired for 90 min. There were no adverse or clinically detectable pharmacologic effects, including no significant changes to vital signs or laboratory results, in any of the subjects. MRI data were acquired on a GE 3.0 T MR750 (Waukesha, WI) for coregistration with PET (Lao et al., 2017).

2.7 | Image analysis

The PMOD software was used to normalize rat PET images to the standard space described by the stereotaxic coordinates (Paxinos & Watson, 2006) via coregistration to an MRI rat template (Schweinhardt, Fransson, Olson, Spenger, & Andersson, 2003; Bieszczad et al., 2012). Mouse PET images were coregistered to a MRI mouse brain template (Ma et al., 2005; Constantinescu et al., 2013) of size $192 \times 96 \times 256$ voxels with a voxel size of 2 mm, which was preliminarily scaled by a factor of 20. The placing of the volume of interests

(VOIs) was guided by examination of the Paxinos and Watson rat atlas. All VOIs were copied to the PET images and time activity curves (TACs) were extracted for each VOI from the dynamic PET data. No additional partial volume correction was applied. Kinetic analysis of rat and mouse *in vivo* PET studies was performed using kinetic analysis toolbox in PMOD. Distribution volume ratio (DVR) in each selected brain region was calculated for using Logan noninvasive method (Logan et al., 1996). Nondisplaceable binding potential (BP_{ND}) was calculated as "DVR-1" (further details described in Kant et al., 2011).

For monkeys, raw list mode data from all scans were summed into 23 frames with corrections applied for scanner dead time and random coincidence events. Sinograms of the emission scan were reconstructed using filtered back-projection (0.5 cm^{-1} ramp filter) with corrections to account for attenuation, scatter, radioactive decay, and scanner normalization to a final matrix size of $128 \times 128 \times 63$ and voxel dimensions of $1.90 \times 1.90 \times 1.21$ mm^3. Circular regions of interest (ROIs) were drawn in various regions of the brain to extract time-activity curves of the radiotracer in the tissue, which included the brain regions of the cerebellum, thalamus, lateral geniculate, and cortex and BP_{ND} were obtained (further details described in Hillmer et al., 2011).

For humans, PET data were histogrammed into frames of 8×0.5 min, 3×2 min, 10×5 min, and 6×10 min. Sinogram data were then reconstructed with a filtered back projection algorithm (Direct Inverse Fourier Transformation; DIFT) using a 4 mm Gaussian filter and included corrections for random events, dead time, signal attenuation, and scanner normalization. Regions of interest were defined with Free-Surfer 5.3 software (http://surfer.nmr.mgh.harvard.edu). Time activity curves were extracted from all regions for subsequent analysis. To quantify specific [^{18}F]Nifene binding, parametric distribution volume ratio (DVR) images were generated using MRTM2 using corpus callosum as reference region, which has been used in previous studies with negligible [^{18}F]2-FA-85380-specific binding (Brody et al., 2006; Meyer et al., 2009). Using PMOD, summed DVR coregistered [^{18}F] Nifene PET image was used along with the MR to identify thalamic radiations of [^{18}F]Nifene (further details described in Lao et al., 2017).

3 | RESULTS

3.1 | ^{18}F-Nifene Synthesis

The radiosynthesis of [^{18}F]Nifene involved a two-step automated procedure, displacement of the aromatic nitro group with [^{18}F]fluoride followed by deprotection of the protecting group (Pichika et al., 2006; Hillmer et al., 2011). Use of alternate trimethylammonium precursor instead of the nitro-precursor for reducing overall radiosynthesis time is currently underway (Patel, Liang, & Mukherjee 2016). The trimethlammonium precursor route is currently used for the radiosynthesis of related [^{18}F]2-FA85380 (Horti et al., 2013) and [^{18}F]flubatine (Sabri et al., 2015).

3.2 | In Vitro Binding Selectivity

Nifene exhibited subnanomolar affinities for the hα2β2 (0.34 nM), hα3β2 (0.80 nM) and hα4β2 (0.83 nM) nAChR and were approximately an order of magnitude better than those

measured for nicotine (Figure 2). For the hβ4 nAChR subtypes, the affinities of both Nifene and nicotine were similar and in the range of 27–219 nM with a potency order of hα4β4> hα2β4> hα4β4 for both Nifene and nicotine (Figure 3). Nifene exhibited weak affinity (169 nM) for the hα7 nAChR (Table 1). Affinity of Nifene and nicotine for rat brain β2 nAChR measured using [^{3}H]cytisine were similar to affinities for the human β2 nAChR. For all other receptor subtypes tested, Nifene did not exhibit significant affinity at 10 μM concentration.

3.3 | Functional Properties

In comparison to 100% agonist activity ([^{86}Rb$^+$]rubidium efflux) of nicotine at 100 μM for the α4β2 receptor subtype, Nifene was found to have only 14% agonist activity at 100 μM (Table 2). The agonist character of Nifene was greater at the α3β4 receptor subtype with 35% compared to nicotine at the same concentration. Nifene exhibited antagonist activities with 18% and 9% inhibition at 1 μM concentration at α4β2 and α3β4 subtypes, respectively. This antagonist activity increased to >50% at 100 μM Nifene concentration. The antagonist activity was defined as inhibiting [^{86}Rb$^+$]rubidium efflux stimulated by 100 μM nicotine at both α4β2 and α3β4 subtypes (Table 2).

3.4 | Acute Toxicity

There were no morbidity or mortality observed in any animals treated with the vehicle control or Nifene, and all animals survived to their scheduled necropsy with minimal clinical observations. No findings associated with Nifene treatment were observed for in-life evaluations of body weight, food consumption, ophthalmology, clinical pathology, urinalysis, and organ weight parameters. Microscopic evaluation of tissues presented no findings associated with Nifene treatment. Intravenous injections of Nifene were well tolerated in Sprague-Dawley male and female rats. Histopathology evaluation on days 6 and 20 presented no dose-related findings from treatment of Nifene. Based on these findings the maximum tolerated dose (MTD) and the no observed adverse effect level (NOAEL) are estimated to exceed 40 μg/kg/day (278 μg/m^2/day), the maximum dose level tested in this study. Molar activities of [^{18}F]Nifene have exceeded >70 GBq/μmol (>2 Ci/μmol), which for a 185 MBq (5 mCi) human dose injection amounts to a total Nifene mass of less than 0.5 μg and well below the MTD and NOAEL for Nifene. The total mass injected in our human studies with ^{18}F-Nifene per injection was <0.10 μg (Lao et al., 2017).

3.5 | Human PET Studies

As reported by Lao et al. (2017), [^{18}F]Nifene was well tolerated in all the human subjects with no adverse side effects. Brain uptake of [^{18}F] Nifene was consistent with α4β2* receptors found in the different regions across all the human subjects. Thalamus and lateral geniculate (LG) had the highest binding followed by the various extrathalamic regions (Figure 4a–c). Significant uptake of [^{18}F]Nifene was also observed in the pituitary of all the subjects with average DVR values of 1.57 for females and 1.45 for males. Since Nifene shows high affinity for the three β2 receptor subtypes, α2, α3 and α4, a more careful brain regional analysis was carried out in attempts to identify specific binding of [^{18}F]Nifene in selected brain regions reported to contain the different receptor subtypes.

α2β2 subtype—Brain regions containing this receptor subtype include interpeduncular nucleus (IPN), olfactory bulb and other cortical regions in rodents (Whiteaker et al., 2009). Using nicotine and α2-knock-out mice, it has been shown that hippocampal α2 receptors may have a role to play in long-term potentiation (Nakauchi, Brennan, Boulter, & Sumikawa, 2007). Significant binding of [^{18}F]Nifene was found in the olfactory gyri with average DVR values of 1.41 for females and 1.31 for males (OG; Figure 4d–h). Binding in the IPN regions (Figure 5e–g) was observed, although exact confirmation of this binding in the midbrain regions is difficult to ascertain due to limits of resolution. However, this binding is ventral to the [^{18}F]Nifene binding measured in substantia niga/ventral tegmental area (SN/VTA) and LG (Figure 5a, b). Extent of [^{18}F]Nifene IPN binding was lower than SN/VTA. The red nucleus exhibited significant binding with average DVR values of 1.73 for females and 1.56 for males, and may be reflective of α2β2 binding based on nonhuman primate observations of exclusive α2 subunits in the red nucleus (Han et al., 2000; Zoli, Pistillo, & Gotti, 2015).

α3β2 subtype—Habenula has been reported to contain significant levels of α3β2 receptor subtype. Using PET/MR coregistered images (Figure 6), low levels of [^{18}F]Nifene binding was identified just below the 3rd ventricle and posterior to SN/VTA. This anatomical location of the habenula is consistent with previous MRI findings in the human brain (Savitz et al., 2011). The habenular volume in each hemisphere is approximately 17–20 mm^3 (Savitz et al., 2011), and may be difficult to accurately assess using the resolution of human HR+ PET scanner (resolution of 4.5 mm). Compared to the substantia nigra whose volume in the normal human brain is approximately 211 mm^3 (Massey et al., 2017), habenula is significantly smaller. Similarly, the VTA is significantly smaller than SN (Murty et al., 2014).

α4β2 subtype—This subtype is most abundant in the brain and found in thalamus, LG, cortical areas, cerebellum and other regions. The binding in SN/VTA is almost similar to the levels seen in red nucleus and may be reflective of α4β2 and α2β2 binding, respectively, in these brain regions. [^{18}F]Nifene was able to identify all these brain regions as seen in Figures 4–6 and described in detail in Lao et al. (2017).

3.6 | Thalamocortical Radiations

At least four types of thalamocortical radiations were observed with [^{18}F]Nifene in the human brain (Figure 7; Thomas et al., 2005). These include anterior thalamic radiation (ATR), superior thalamic radiation (STR), inferior thalamic radiation (ITR), and posterior thalamic radiation (PTR) as shown in the schematic in Figure 7a. Emerging from the anterior thalamus, ATR appears prominently extending to the cortical regions via the white matter tracts in the internal capsule between the caudate and putamen as seen in the coronal slices (Figure 7b, c) and in the transaxial slices (Figure 7i, j) with average DVR values of 1.67 for females and 1.58 for males. Superior thalamic radiations (STR, Figure 7e, f) project upward to distinct white matter tracts in superior longitudinal fasciculus (SLF) with [^{18}F]Nifene average DVR values of 1.55 for females and 1.38 for males in SLF (Figure 7g). SLF has connections to frontal, temporal, and occipital cortex (Kochunov et al., 2013). Inferior thalamic radiations (ITR) project to the auditory cortex and limbic regions as shown

in Figure 7e,i. Posterior thalamic radiations (PTR) extend to the occipital cortex as well as regions of the posterior cingulate cortex (PCC) as seen in Figure 7d.

3.7 | Aging Effects

Age and gender of all the subjects and the distribution volume ratios (DVR) in brain regions are summarized in Table 3. Age spanned 5 decades in both male and female subjects. Thalamus exhibited the highest DVR values in both the genders with no significant change with aging. Similarly, in other brain regions, lateral geniculate and SN/VTA also did not exhibit any age-related effects. Greater variation were found in the DVR values of frontal cortex and cerebellum (showing an increase with age), however, significance of this will require a larger number of subjects.

3.8 | Gender Effects

There were significant differences between male and female in the various brain regions. Female subjects showed higher DVR values compared to males in all the brain regions that were evaluated. In the thalamus, females had an average DVR of 2.58 ±0.11 while males had 2.24 ±0.10, which is 15% higher in females compared to males (p-value of 0.004). Similarly, in LG, females had an average DVR of 2.46 ± 0.07 while males had 2.17 ±0.08, which is 13% higher in females compared to males (p-value of 0.001). Substantia nigra/VTA showed a DVR

4 | DISCUSSION

Nifene was designed to be structurally similar to nicotine, containing the pyridine ring and the 5-membered unsaturated 3,4-dehydropyrrolidine ring (Figure 1b) so that the basicity of the nitrogen would be lowered (Pichika et al., 2006). It has been suggested that tryptophan residue 149 in the α4β2* receptor may be involved in a strong cation-π interaction with nicotine and is conserved in the different species (Xiu, Puskar, Shanata, Lester, & Dougherty, 2009). Modulation of this cation-π interaction may play a role in the faster clearance of [18F]Nifene from various brain regions in the different species (Kant et al., 2011; Hillmer et al., 2011; Lao et al., 2017) compared to the related azetidine-ring containing [18F] 2-FA-85380. This feature of faster kinetics induced by 3,4-dehydropyrrolidine ring compared to the azetidine ring was further evidenced by the otherwise structurally identical PET radiotracers, nifrolene versus nifzetidine (Pichika et al., 2011; Pichika et al., 2013).

Across the various species, [18F]Nifene exhibited selective targeting to α4β2* receptors, lack of toxicity, suitable dosimetry, rapid kinetics, quantifiable in PET studies, with the potential of becoming available for large multicenter trials. As previously discussed for [18F] Mefway (Mukherjee et al., 2016), such properties facilitate the translation of [18F]Nifene to human research and clinical studies.

In human nAChR clones, overall affinity of Nifene was found to be higher than nicotine as summarized in Table 1. Nifene was found to have high affinity for the three hβ2 nAChR subtypes (α2>α3 α4). Our previous studies with [18F]Nifene in β2 knock-out mice brains revealed little specific binding compared to the wild-type mice (Bieszczad et al., 2012). This

is consistent with the weaker affinities of Nifene for β4 and α7 nAChR subtypes. Thus, in PET studies of animal models and humans, [^{18}F]Nifene binding is predominantly reflective of binding to β2 nAChR. Histochemical mRNA hybridization studies in rat brain show subunit concentration levels: β2>α4>α3>α2, of which α4β2 nAChR being the major subtype (Wada et al., 1989). In the nonhuman primate however, the order is β2>α4>α2>α3, with significantly higher levels of α2 compared to rats (Han et al., 2000). Interestingly, it must be noted that while Nifene had an order of magnitude better affinity for the hβ2 nAChR subtypes compared to nicotine, their affinities for the hβ4 nAChR subtypes were similar.

In functional assays, compared to nicotine, Nifene was found to exhibit greater antagonist properties at 100 μM concentrations compared to agonist properties (Table 2). The small difference in structure between nicotine and Nifene (Figure 1) causes a dramatic change in their functional properties. Previous reports on pyridylether derivatives have shown a change from agonist to antagonist character when substituent groups, such as a propyl or butyl group are included at the 5-position of the pyridine ring (Lin et al, 1998). This structure-activity relationship was considered when we designed the fluoroalkyl derivatives as putative antagonists (Chattopadhyay et al., 2005; Pichika et al., 2013). Our findings with Nifene which has a small fluorine atom at the 2-position in the pyridine ring without a fluoropropyl group was unexpected. The large electronic effects of fluorine, both spatial and inductive, may be causing a shift in its functional properties. Thus, Nifene may be characterized as a partial agonist. It should be noted that varen-cline, the smoking cessation drug is also known to be a partial agonist and has 30–60% in vivo efficacy compared to nicotine (Niaura, Jones, & Kirkpatrick, 2006).

The calculated Nifene human equivalent dose (HED) based on our rat toxicity NOAEL results at 40 μg/kg/day =6.49–7.57 μg/kg [40 μg/kg (Animal dose) × (6–7 (Rat Km)/37 (Human Km)]. Specific activities of [^{18}F]Nifene for all our studies have exceeded >70 GBq/μmol (>2 Ci/μmol), which for a 185 MBq (5 mCi) human dose injection amounts to a total Nifene mass of less than 0.50 μg which is well below the NOAEL for Nifene. The mass injected in our human studies with [^{18}F] Nifene was approximately 0.05 μg (Lao et al., 2017). Thus, the total mass of Nifene administered in PET studies is 10^3–10^4 times less than the NOAEL of approximately 7 μg/kg, HED. Previous reports on related PET agent [^{18}F]2-FA-85380 showed some pharmacological effects in mice at >3 μmol/kg (or >0.5 mg/kg) which is significantly greater than doses used in PET studies (Vaupel et al., 2005). There were no adverse effects with [^{18}F]2-FA-85380 up to 10 pmol/kg and suggested that 4 PET studies of 185 MBq (5 mCi) per injection could be carried out in human volunteers (Kimes et al., 2003). Human radiation dosimetry studies with [^{18}F]Nifene show similarities with our reported mice radiation dosimetry findings with urinary bladder as the critical organ (Constantinescu et al., 2013; Betthauser et al., 2017). Annually, at least 4 human PET studies of 185 MBq (5 mCi) per injection of [^{18}F]Nifene may be carried out (Betthauser et al., 2017).

Human brain PET studies of [^{18}F]Nifene showed high levels of binding in the thalamus with lower levels in the cortical and midbrain regions (Lao et al., 2017) (Supporting Figure 1). This is generally consistent with the reported postmortem human brain distribution of

nAChR using [3H]epibatidine and [3H]nicotine (Marutle, Warpman, Bogdanovic, & Nordberg, 1998) and distribution of binding of other PET radiotracers for this receptor system (Kuwabara et al., 2016). Pituitary gland also exhibited significant binding of [18F]Nifene and was the region with the largest variation in measured DVR values amongst the 8 subjects (Table 3). The hypothalamus–pituitary–adrenal (HPA) axis has been known to be involved in various physiological responses, including stress, mood disorders, and others (Bertrand, 2005). The HPA axis is stimulated by nicotine and smoking resulting in the increase of ACTH and cortisol (Tweed, Hsia, Lufty, & Friedman, 2012). Interaction of nicotine at the nAChRs both in the hypothalamus and pituitary as well as other brain regions may be involved in this endocrine effect (Zemkova, Kucka, Bjelobaba, Tomic, & Stojilkovic, 2013).

The habenula has been shown to play a role in nicotine withdrawal signs and other properties of nicotine (Baldwin, Alanis, & Salas, 2011). In the nonhuman primate, mRNA for the α3 subtype (both α3β4 and α3β2) have been found in greater amounts compared to other subtypes in the habenula (Han et al, 2000). Affinity of Nifene for the α3β4 subtype is 190 nM, and with this weak affinity it is unlikely [18F]Nifene will have significant retention for imaging purposes. However, for α3β2 subtype Nifene has an affinity of 0.80 nM which is more suitable for in vivo imaging. Thus, images of [18F]Nifene binding in the habenula may reflect α3β2 binding. Delineation of the binding of [18F]Nifene is made difficult due to the small size of the human habenula (Figure 6b). Additionally, because of the spillover effects from the SN/VTA, the measurement may be further confounded. It has been postulated that antagonists for α3β4 acting on the habenula may have a role in smoking cessation (Harrington et al., 2016). It must be noted that Nifene has a >50% antagonist character for the α3β4 subtype (Table 2).

Since Nifene showed the highest affinity for the α2β2 subtype, brain regions with potentially significant levels of this subtype were examined. Although human postmortem data is not available on the distribution of this receptor subtype, information from the rodent models suggest at least two prominent areas, IPN and olfactory bulb which may contain higher α2 receptor levels (Whiteaker et al., 2009). Subtypes of nAChR in habenula and IPN have been a subject to understand brain responses to nicotine (Antolin-Fontes, Ables, Gorlich, & Ibanez-Tallon, 2015). Nonhuman primates have greater levels of this receptor subtype in the various brain regions, including the thalamus (Han et al., 2000). Clear demarcation and quantification of IPN in the human midbrain is challenging due to the adjacent SN/VTA. Postmortem human brain autoradiography using [3H]nicotine shows significant binding in IPN (Duncan et al., 2008). Monkey brain autoradiograms showed IPN binding of [3H]epibatidine (Han et al., 2003). The red nucleus appears to be lacking α4, but contains the α2 subtype (Han et al., 2000). Thus, if the nonhuman primate findings hold true in humans (Machaalani et al., 2010), [18F]Nifene in the red nucleus may reflect α2β2 receptor subtype binding. Figure 5e–g shows distinct bilateral binding of [18F]Nifene in the red nucleus region. The red nucleus has been implicated in locomotor, gait, language and other functions (Garzon, Sitnikov, Backman, & Kalpouzos, 2017). The olfactory gyri were more clearly visualized and the levels of [18F]Nifene binding were similar to the cortical regions. Although Nifene has an approximately 5-fold higher affinity for α2β2 compared to α3β2 and α4β2 subtypes, it may be necessary to enhance this selectivity in favor of α2β2 in

order to more clearly identify brain regions containing this receptor subtype. The increasing significance of the α2β2 subtype suggests a need for a more selective PET radiotracer for this receptor subtype.

Nicotinic acetylcholinergic receptors have now been shown to play a critical role in brain connectivity through nonsynaptic transmission (Lendvai & Sylvester, 2008). In a preliminary study, the binding of a PET radiotracer to the human brain white matter was observed (Ding et al., 2004). Recent studies on the effect of nicotine using DTI have found activation of several white matter tracts further suggesting a CNS role of non-neuronal nicotinic receptors (Kochunov et al., 2013; Yu et al., 2016). Thalamocortical radiations in the white matter tracts have been reported to play a critical role in brain injury (Thomas et al., 2005) and motor and verbal memory (Philip, Korgaonkar, & Grieve, 2014). The anterior thalamic radiation (ATR) exhibited distinct and significant [^{18}F]Nifene binding projecting from the thalamus, between the caudate and putamen to the frontal cortical areas. These tracts from the cortical areas via the thalamus down to the spinal cord white matter regions play a very important role in signal transduction. The superior thalamic radiation (STR) fans out upwards from the thalamus interconnecting various cortical regions. It also clearly forms a white matter tract, SLF which interconnects frontal and temporal regions. Fractional anisotropy in SLF was distinctly affected upon nicotine patch treatment in DTI studies compared to placebo (Kochunov et al., 2013), in adolescent/young adult smokers (Gogliettino, Potenza, & Yip, 2016), and lesions smokers in clinically isolated syndrome, a demyelinating disorder, a precursor to multiple sclerosis (Durhan et al., 2016). Inferior thalamic radiations (ITR) project to the temporal cortex including auditory cortex where auditory projections from medial geniculate nucleus have been studied using fMRI and diffusion tractography (Javed et al., 2014). Our findings suggest that these thalamic radiations have significant amounts of α4β2* nAChR as demonstrated by [^{18}F]Nifene binding.

There have been few animal studies on the effects of aging on α4β2* nAChRs. A detailed autoradiographic study in rats (2-month old vs. 20-month old) did not find a change in nAChR (Tribollet, Bertrand, Marguerat, & Raggenbass, 2004). Other mice studies have shown either no change or a small decrease in receptor concentrations in select brain regions with aging (Rogers, Gahring, Collins, & Marks, 1998; Ferrari, Pedrazzi, Algeri, Agnati, & Zoli, 1999; Picciotto & Zoli, 2002). Postmortem human brain studies revealed an age-related reduction in the binding of (±)-[^{3}H]epibatidine in frontal and temporal cortex (Marutle et al., 1998). Aging effects in human PET studies of this receptor using [^{18}F]2-FA-85380 suggest a weak association between aging and α4β2* nAChR (Meyer et al., 2009). However, in a single photon emission computed tomography (SPECT) study using [^{123}I]5-IA-85380 and scan time of 8 hr, a 2.4–4.8% per decade decrease in [^{123}I]5-IA-85380 has been reported (Mitsis et al., 2009). In this preliminary human study with [^{18}F]Nifene, no significant changes were observed in the binding of ^{18}F-Nifene across several decades in males and females. Figure 8 shows DVR values of thalamic and extrathalamic brain regions over 5 decades with no significant change in receptor levels. As reported previously, these measures of individual subjects were confirmed by retest studies on the same subjects (Lao et al., 2017). Differences in kinetics of in vivo binding between [^{123}I]5-IA-85380 and [^{18}F] Nifene and potential issues of cellular trafficking of nAChRs (St john, 2009) may have to be

considered in order to ascertain that the two radiotracers are measuring the same population of β2* nAChRs.

In contrast to the α4β2* nAChRs, studies on dopamine D2/D3 receptors have shown a progressive loss with aging in humans. A number of studies using PET employing a variety of radiopharmaceuticals show a lowering in D2/D3 receptor concentrations in all brain regions. These studies indicate that the loss of D2/D3 receptors may be approximately 6–13% per decade (Mukherjee et al., 2002). Using our previously published data on D2/D3 receptors on a separate group of subjects (Mukherjee et al., 2002), both thalamus and substantia nigra/ventral tegmental area show a decline with aging (Figure 8b), whereas α4β2* nAChR in the present study do not exhibit any significant change due to aging in these regions. The selective sparing of α4β2* nAChR is noteworthy, since it has been suggested that the loss of D2/D3 receptors may be from degeneration of neurons due to progressive free radical damage to cells, loss of proteins due to inefficient recycling, decrease in D2 receptor gene transcription, cell death, etc. (Semsei, 2000; Tohgi, Utsugisawa, Yoshimura, Nagane, & Mihara 1998). This decrease in D2/D3 receptors may be manifested in neuropsychological, cognitive and motor function deficits in the aging population (Volkow et al., 1998).

Gender differences were observed in this small study with the female subjects showing higher [18F]Nifene DVR values (Table 3). In the thalamus, lateral geniculate and SN/VTA, females showed a 9–15% higher [18F]Nifene binding and were found to be significant (p <0.05). This finding is consistent with the higher binding of [123I]5-IA-85380 in female nonsmokers compared to male nonsmokers measured in a SPECT study (Cosgrove, Esterlis, Sandiego, Petrulli, & Morris, 2012) and in a PET study using [18F]2-FA-85380 (Meyer et al., 2009). A faster brain nicotine accumulation has been reported in the case of females versus males (Zuo et al., 2015) and higher activation of brain regions to smoking cues in females has also been observed (Zanchi, Brody, Borgwardt, & Haller, 2016). Since females have a greater neuropharmacological response to nicotine compared to males (references cited in Zuo et al., 2015), it remains to be seen if the higher DVR in females is a contributing factor to the female-male differences, including the higher relapse seen in females (e.g., Xu et al., 2008). Smoking had divergent effects on the binding of [123I]5-IA-85380 in females versus males; females showed little effect while males showed increased [123I]5-IA-85380 binding compared to nonsmokers (Cosgrove et al., 2012). A number of PET and SPECT imaging studies have been carried out to further understand the molecular/cellular mechanisms underlying these differences (see reviews, Jasinka, Zodrick, Brody, & Stein, 2014; Cosgrove et al., 2015). Since it has been suggested that [18F]2-FA-85380 (and perhaps [123I]5-IA-85380) provide measures of both intracellular and cell surface bound α4β2* receptors (Lester et al., 2009), fast acting [18F]Nifene may be less amenable to intracellular localization and thus provide information on cell surface receptors only. A larger study with [18F]Nifene to further confirm female-male differences in the α4β2* receptor levels will be valuable and further studies need to be carried out in order to delineate subcellular nature of the binding of these radiotracers.

[18F]Nifene was taken up rapidly in brain regions across all species and was shown to be the only radioactive component in the rat brain after intravenous administration (Kant et al.,

2011). Excellent test-retest results in all the species demonstrates the reliability of [^{18}F] Nifene studies. Ratio of brain regions versus cerebellum (except in humans where corpus callosum was used) reached a plateau approximately 40 min post-injection in the various species suggestive of pseudo-equilibrium in vivo. Thus, based on the kinetics of [^{18}F]Nifene, a scan time of 40 min may be appropriate across the various species in order to derive reliable quantitative data.

The binding affinity of Nifene was similar in rat and human (Table 1). [^{18}F]Nifene binding to brain tissue of various species was similar and in agreement with the inter-species homology of the α4β2* receptors. The absence of any significant [^{18}F]Nifene in our previous β2* knock-out mice studies further confirmed α4β2* binding of [^{18}F]Nifene (Bieszczad et al., 2012). Thalamus across the various species exhibited the highest level of binding of [^{18}F]Nifene, whereas the cerebellum in the rodents and nonhuman primates was the lowest. Human cerebellum was an exception which showed higher binding while corpus callosum was the least (Lao et al., 2017). In our rat studies, amongst the white matter regions investigated, corpus callosum had the least amount of [^{18}F]Nifene binding (Bieszczad et al., 2012). As seen in Figure 9, [^{18}F]Nifene did not exhibit extracranial uptake binding in the various species, thus indicative of the stability of [^{18}F]Nifene to defluorination during the course of a PET scan. Ratio of thalamus to cerebellum or corpus callosum (in the case of humans) was as follows: mouse =2; rat =3.1; monkeys =3.2 and humans =2.6. Further studies are required in rodents and nonhuman primates in order to assess aging effects and gender effects with [^{18}F]Nifene.

Following are some of the limitations of the study: (1) The number of subjects were only 8. In order to ascertain an aging effect and the presence of a gender effect, a larger [^{18}F]Nifene study with male and female subjects will have to be carried out and should include >70 year-old subjects; (2) The use of corpus callosum as a reference region for [^{18}F]Nifene PET studies needs to be established by carrying out nicotine challenge studies. If corpus callosum has non-negligible [^{18}F] Nifene specific binding, it would underestimate DVR and may have an effect on age- and gender differences reported here.

5 | CONCLUSION

[^{18}F]Nifene is an effective nAChR α4β2* receptor imaging agent in humans. Ability of [^{18}F]Nifene to identify thalamic radiations to various brain regions is highly significant in order to understand the role of white matter in neurodegeneration. The presence of a significant gender effect may help understand the prominent female-male differences in smokers and addiction. Our findings with [^{18}F]Nifene across species provides evidence of similarity and dissimilarity in the brain distribution of nAChR α4β2* across species which is vital for translational research. Thus, [^{18}F]Nifene may be reliably used to quantify nAChR α4β2* receptor distribution in brain regions for the study of various CNS disorders.

Supplementary Material

Refer to Web version on PubMed Central for supplementary material.

Acknowledgments

References

Albuquerque EX, Pereira EFR, Alkondon M, Rogers SW. Mammalian nicotinic acetylcholine receptors: from structure to function. Physiological Review. 2009; 89:73–120.

Antolin-Fontes B, Ables JL, Gorlich A, Ibanez-Tallon I. The habenulo-interpeduncular pathway in nicotine aversion and withdrawal. Neuropharmacology. 2015; 96:213–222. [PubMed: 25476971]

Baldwin PR, Alanis R, Salas R. The role of the habenula in nicotine addiction. Journal of Addiction Research and Therapy. 2011 S1–002.

Bieszczad KM, Kant R, Constantinescu CC, Pandey SK, Kawai HD, Metherate R, … Mukherjee J. Nicotinic acetylcholine receptors in rat forebrain that bind ^{18}F-nifene: relating PET imaging, autoradiography, and behavior. Synapse. 2012; 66:418–434. [PubMed: 22213342]

Betthauser, TJ., Hillmer, AT., Lao, PJ., Ehlerding, E., Mukherjee, J., Stone, CK., Christian, BT. Human biodistribution and dosimetry of [18F]Nifene, an α4β2* nicotinic acetylcholine receptor PET tracer. Nuclear Medicine and Biology. 2017. https://doi.org/10.1016/j.nucmedbio.2017.08.001

Bertrand D. The possible contribution of neuronal nicotinic acetylcholine receptors in depression. Dialogues Clinical Neuroscience. 2005; 7:207–216.

Brody AL, Mandelkern MA, London ED, Olmstead RE, Farahi J, Scheibal D, … Mukhin AG. Cigarette smoking saturates brain alpha4beta2 nicotinic acetylcholine receptors. Archives General Psychiatry. 2006; 63:907–915.

Brody AL, Mandelkern MA, Costello MR, Abrams AL, Scheibal D, Farahi J, … Mukhin AG. Brain nicotinic acetylcholine receptor occupancy: effect of smoking a denicotinized cigarette. International Journal Neuropsychopharmacology. 2009; 12:305–316.

Chattopadhyay S, Xue B, Pichika R, Collins D, Bagnera R, Leslie FM, … Mukherjee J. Synthesis and evaluation of nicotine α4β2 receptor ligand, 5-(3′-fluoropropyl)-3-(2-(S)-pyrrolidinyl) methoxy)pyridine (^{18}F-nifrolidine) in rodents and imaging by PET in non-human primate. Journal of Nuclear Medicine. 2005; 46:130–140. [PubMed: 15632043]

Cho ZH, Law M, Chi JG, Choi SH, Park SY, Kammen A, … Kim Y-B. An anatomic review of thalamolimbic fiber tractography: Ultra-high resolution direct visualization of thalamolimbic fibers anterior thalamic radiation, superolateral and inferomedial medial forebrain bundles, and newly identified septum pellucidum tract. World Neurosurgery. 2015; 83:54–61. [PubMed: 23973452]

Cosgrove KP, Esterlis I, McKee SA, Bois F, Seibyl JP, Mazure CM, … O'Malley SS. Sex differences in availability of β2*-nicotinic acetylcholine receptors in recently abstinent tobacco smokers. Archives in General Psychiatry. 2012; 69:418–427.

Cosgrove, KP., Esterlis, I., Sandiego, C., Petrulli, R., Morris, ED. Imaging tobacco smoking with PET and SPECT. In: Balfour, DJK., Munafo, MR., editors. The neuropharmacology of nicotine, Current Topics in Behavioral Neurosciences. Vol. 24. Switzerland: Springer International Publishing; 2015. p. 1-17.

Constantinescu CC, Garcia A, Mirbolooki MR, Pan ML, Mukherjee J. Evaluation of [18F]Nifene biodistribution and dosimetry based on whole-body PET imaging of mice. Nuclear Medicine and Biology. 2013; 40:289–294. [PubMed: 23265670]

Constantinescu CC, Mukherjee J. Performance evaluation of an Inveon PET preclinical scanner. Physics in Medicine and Biology. 2009; 54:2885–2899. [PubMed: 19384008]

Declercq, LD., Vandenberghe, R., Von Laere, K., Verbruggen, A., Bormans, G. Drug development in Alzheimers disease: The contribution of PET and SPECT. Frontiers in Pharmacology. 2016. https://doi.org/10.3389/fphar.2016.00088

Ding YS, Fowler J, Logan J, Wang GJ, Telang F, Garza V, … Vocci F. 6-[18F]Fluoro-A-85380, a new PET tracer for the nicotinic acetylcholine receptor: studies in the human brain and in vivo demonstration of specific binding in the white matter. Synapse. 2004; 53:184–189. [PubMed: 15236351]

D'Souza MS. Neuroscience of nicotine for addiction medicine: novel targets for smoking cessation medications. Progress in Brain Research. 2016; 223:191–214. [PubMed: 26806777]

Duncan JR, Randall LL, Belliveau RA, Trachtenberg FL, Randall B, Habbie D, … Kinney HC. The effect of maternal smoking and drinking during pregnancy upon 3H-nicotine receptor brainstem binding in infants dying of the sudden infant death síndrome: Initial observations in a high risk population. Brain Pathology. 2008; 18:21–31. [PubMed: 17924983]

Durhan G, Diker S, Has AC, Karakaya J, Kume AT, Oguz KK. Influence of cigarette smoking on white matter in patients with clinically isolated syndrome as detected by diffusion tensor imaging. Diagnostic and Interventional Radiology. 2016; 22:291–296. [PubMed: 27015443]

Easwaramoorthy B, Pichika R, Collins D, Potkin SG, Leslie FM, Mukherjee J. Effect of acetylcholinesterase inhibitors on the binding of nicotinic alpha4beta2 receptor PET radiotracer, (18)F-nifene: A measure of acetylcholine competition. Synapse. 2007; 61:29–36. [PubMed: 17068780]

Ferrari R, Pedrazzi P, Algeri S, Agnati LF, Zoli M. Subunit and region-specific decreases in nicotinic acetylcholine receptor mRNA in the aged rat brain. Neurobiology of Aging. 1999; 20:37–46. [PubMed: 10466891]

Garg PK, Lokitz SJ, Nazih R, Garg S. Biodistribution and radiation dosimetry of 11C-nicotine from whole body PET imaging in humans. Journal of Nuclear Medicine. 2017; 58:473–478. [PubMed: 27660145]

Garzon, B., Sitnikov, R., Backman, L., Kalpouzos, G. Automated segmentation of midbrain structures with high iron content. Neuro-image. 2017. https://doi.org/10.1016/j.neuroimage.2017.06.016

Gogliettino A, Potenza MN, Yip SW. White matter development and tobacco smoking in young adults: A systematic review with recommendations for future research. Drug and Alcohol Dependence. 2016; 162:26–33. [PubMed: 26948756]

Han Z-Y, Le Novere N, Zoli M, Hill JA Jr, Champtiaux N, Changeux JP. Localization of nAChR subunit mRNAs in the brain of Macaca mulatta. European Journal of Neuroscience. 2000; 12:3664–3674. [PubMed: 11029636]

Han ZY, Zoli M, Cardona A, Bourgeois JP, Changeux JP, Le Novere N. Localization of [3]nicotine, [3H]cytisine, [3H]epibatidine, and [125I]a-bungaratoxin binding sites in the brain of Macaca mulatta. Journal of Comparative Neurology. 2003; 461:49–60. [PubMed: 12722104]

Harrington L, Vinals X, Herrera-Solis A, Flores A, Morel C, Tolu S, … Robledo P. Role of β4* nicotinic acetylcholine receptors in the habenulo-interpedncular pathway in nicotine reinforcement in mice. Neuropsychopharmacolgy. 2016; 41:1790–1802.

Hillmer AT, Wooten DW, Slesarev MS, Ahlers EO, Barnhart TE, Schneider ML, … Christian BT. Measuring α4β2* nicotinic acetylcholine receptor density in vivo with [(18)F]nifene PET in the nonhuman primate. Journal of Cerebral Blood Flow and Metabolism. 2013; 33:1806–1814. [PubMed: 23942367]

Hillmer AT, Wooten DW, Moirano JM, Slesarev M, Barnhart TE, Engle JW, … Christian BT. Specific α4β2 nicotinic acetylcholine receptor binding of [F-18]nifene in the rhesus monkey. Synapse. 2011; 65:1309–1318. [PubMed: 21674627]

Horti AG, Kuwabara H, Holt DP, Dannals RF, Wong DF. Recent PET radioligands with optimal brain kinetics for imaging nicotinic acetylcholine receptors. Journal of Labelled Compounds and Radiopharmaceuticals. 2013; 56:159–166. [PubMed: 24285321]

Jasinka AJ, Zodrick T, Brody AL, Stein EA. Dual role of nicotine in addition and cognition: A review of neuroimaging studies in humans. Neuropharmacology. 2014; 84:111–122. [PubMed: 23474015]

Javed F, Warren JD, Micallef C, Thornton JS, Golay X, Yousry T, Mancini L. Auditory tracts identified with combined fMRI and diffusion tractography. Neuroimage. 2014; 84:562–574. [PubMed: 24051357]

Kant R, Constantinescu CC, Parekh P, Pandey SK, Pan ML, Easwaramoorthy B, Mukherjee J. Evaluation of 18F-nifene binding to α4β2 nicotinic receptors in the rat brain using microPET imaging. EJNMMI Research. 2011; 1:1.

Kimes AS, Horti AG, London ED, Chefer SI, Contoreggi C, Ernst M, … Mukhin AG. 2–18F-FA-85380: PET imaging of brain nicotinic acetylcholine receptors and whole body distribution in humans. FASEB Journal. 2003; 17:1331–1333. [PubMed: 12759330]

Kochunov P, Du X, Moran LV, Sampath H, Wijtenburg SA, Yang Y, … Hong LE. Acute nicotine administration effects on fractional anisotropy of cerebral white matter and associated attention performance. Frontiers in Pharmacology. 2013; 4:117. [PubMed: 24065920]

Kutlu MG, Parikh V, Gould TJ. Nicotine addiction and psychiatric disorders. International Reviews in Neurobiology. 2015; 124:171–208.

Kuwabara H, Gao Y, Stabin M, Coughlin J, Nimmagadda S, Dannals RF, … Horti AG. Imaging α4β2 nicotinic acetylcholine receptors (nAChRs) in baboons with 18F-XTRA, a radioligand with improved specific binding in extra-thalamic regions. Molecular Imaging and Biology. 2016; 19:280–288.

Lao PJ, Betthauser TJ, Tudorascu DL, Barnhart TE, Hillmer AT, Stone CK, … Christian BT. [18F]Nifene test-retest reproducibility in first-in-human investigations of α4β2* nicotinic acetylcholine receptors. Synapse. 2017; 71:e21981.

Lendvai B, Sylvester E. Nonsynaptic chemical transmission through nicotinic acetylcholine receptors. Physiological Reviews. 2008; 88:333–349. [PubMed: 18391166]

Lester HA, Xiao X, Srinivasan R, Son CD, Miwa J, Pantoja R, … Wang JC. Nicotine is a selective pharmacological chaperone of acetylcholine receptor number and stoichiometry. Implications for drug discovery. The AAPS Journal. 2009; 11:167–177. [PubMed: 19280351]

Lin NH, Gunn DE, Li Y, He Y, Bai H, Ryther KB, … Holladay MW. Synthesis and structure-activity relationships of pyridine-modified analogs of 3-[2((S)-pyrrolidinyl)methoxy]pyridine, A-84543, a potent nicotinic acetylcholine receptor agonist. Bioorganic Medicinal Chemistry Letters. 1998; 8:249–254. [PubMed: 9871663]

Logan J, Fowler JS, Volkow ND, Wang GJ, Ding YS, Alexoff DL. Distribution volume ratios without blood sampling from graphical analysis of PET data. Journal of Cerebral Blood Flow and Metabolism. 1996; 16:834–840. [PubMed: 8784228]

Lombardo S, Maskos U. Role of the nicotinic acetylholine receptor in Alzheimer's disease pathology and treatment. Neuropharmacology. 2015; 96:255–262. [PubMed: 25514383]

Ma Y, Hof PR, Grant SC, Blackband SJ, Bennett R, Slatest L, … Benveniste H. A three-dimensional digital atlas database of the adult C57BL/6J mouse brain by magnetic resonance microscopy. Neuroscience. 2005; 135:1203–1215. [PubMed: 16165303]

Machaalani R, Kashi PK, Waters KA. Distribution of nicotinic acetylcholine receptor subunits α7 and β2 in the human brainstem and hippocampal formation. Journal of Chemical Neuroanatomy. 2010; 40:223–231. [PubMed: 20566330]

Marutle A, Warpman U, Bogdanovic N, Nordberg A. Regional distribution of subtypes of nicotinic receptors in human brain and effect of aging studied by (±)-[3H]epibatidine. Brain Research. 1998; 801:143–149. [PubMed: 9729344]

Massey LA, Miranda MA, Al-Helli O, Parkes HG, Thornton JS, So PW, … Yousry TA. 9.4T MR microscopy of the substantia nigra with pathological validation in controls and disease. Neuroimage: Clinical. 2017; 13:154–163. [PubMed: 27981030]

Meyer PM, Strecker K, Kendziorra K, Becker G, Hesse S, Woelpl D, … Schwarz J. Reduced α4β2*-nicotinic acetylcholine receptor binding and its relationship to mild cognitive and depressive symptoms in Parkinson disease. Archives in General Psychiatry. 2009; 66:866–877.

Mitsis EM, Cosgrove KP, Staley JK, Bois F, Frohlich EB, Tamagnan GD, … van Dyck CH. Age-related decline in nicotinic receptor availability with [123I]5-IA-85380 SPECT. Neurobiology of Aging. 2009; 30:1490–1497. [PubMed: 18242781]

Mukherjee J, Bajwa AK, Wooten DW, Hillmer AT, Pan ML, Pandey SK, … Christian BT. Comparative assessment of ^{18}F-Mefway as a serotonin 5-HT1A receptor PET imaging agent across species-rodents, nonhuman primates and humans. Journal of Comparative Neurology. 2016; 524:1457–1471. [PubMed: 26509362]

Mukherjee J, Christian BT, Dunigan K, Shi B, Narayanan TK, Satter M, Mantil J. Brain Imaging of ^{18}F-fallypride in normal volunteers: Blood analysis, distribution, test-retest studies and preliminary assessment of sensitivity to aging effects on dopamine D-2/D-3 receptors. Synapse. 2002; 46:170–188. [PubMed: 12325044]

Murty VP, Shermohammed M, Smith DV, Carter RM, Huettel SA, Adcock RA. Resting state distinguish human ventral tegmental area from substantia nigra. Neuroimage. 2014; 100:580–589. [PubMed: 24979343]

Nakauchi S, Brennan RJ, Boulter J, Sumikawa K. Nicotine gates long-term potentiation in the hippocampal CA1 region via the activation of alpha2* nicotinic ACh receptors. European Journal of Neuroscience. 2007; 25:2666–2681. [PubMed: 17466021]

Nees F. The nicotinic cholinergic system function in the human brain. Neuropharmacology. 2015; 96:289–301. [PubMed: 25446570]

Niaura R, Jones C, Kirkpatrick P. Varenicline. Nature Reviews Drug Discovery. 2006; 5:537–538.

Nyback H, Halldin C, Ahlin A, Curvall M, Eriksson L. PET studies of the uptake of (S)- and (R)-[11C]nicotine in the human brain: difficulties in visualizing specific receptor binding in vivo. Psychopharmacology. 1994; 115:31–36. [PubMed: 7862909]

Parikh V, Kutlu MG, Gould TJ. nAChR dysfunction as a common substrate for schizophrenia and comorbid nicotine addiction: current trends and perspectives. Schizophrenia Research. 2016; 171:1–15. [PubMed: 26803692]

Patel IH, Liang C, Mukherjee J. New precursor in improved 18F-nifene synthesis for imagingnicotinic receptors. Journal of Nuclear Medicine. 2016; 57(6):1086.

Paxinos, G., Watson, C. The Rat Brain in Stereotaxic Coordinates. New York: Elsevier Press; 2006.

Picciotto MR, Zoli M. Nicotinic receptors in aging and dementia. Journal of Neurobiology. 2002; 53:641–655. [PubMed: 12436427]

Pichika R, Easwaramoorthy B, Collins D, Christian BT, Shi B, Narayanan TK, … Mukherjee J. Nicotinic alpha4beta2 receptor imaging agents: part II. Synthesis and biological evaluation of 2-[18F]fluoro-3-[2-((S)-3-pyrrolinyl)methoxy]pyridine ([^{18}F]nifene) in rodents and imaging by PET in nonhuman primate. Nuclear Medicine and Biology. 2006; 33:295–304. [PubMed: 16631077]

Pichika R, Easwaramoorthy B, Christian BT, Shi B, Narayanan TK, Collins D, Mukherjee J. Nicotine α4β2 receptor imaging agents. Part III. Synthesis and evaluation of [^{18}F]Nifzetidine in rodents and imaging by PET in non-human primate. Nuclear Medicine and Biology. 2011; 38:1183–1192. [PubMed: 21831652]

Pichika R, Kuruvilla SA, Patel N, Vu K, Sinha S, Easwaramoorthy B, … Mukherjee J. Nicotine α4β2 receptor imaging agents. Part IV. Synthesis and evaluation of [^{18}F]Nifrolene in rodents and non-human primate by PET imaging. Nuclear Medicine and Biology. 2013; 40:117–125. [PubMed: 23141552]

Philip DJ, Korgaonkar MS, Grieve SM. Thalamic volume and thalamocortical white matter tracts correlate with motor and verbal memory performance. Neuroimage. 2014; 91:77–83. [PubMed: 24401559]

Quik M, Bordia T, Zhang D, Perez XA. Nicotine and nicotinic receptor drugs:Potential for Parkinson's disease and drug-induced movement disorders. International Reviews in Neurobiology. 2015; 124:247–271. [PubMed: 26472532]

Rogers SW, Gahring LC, Collins AC, Marks M. Age-related changes in neuronal nicotinic acetylcholine receptor subunit a4 expression are modified by long-term nicotine administration. Journal of Neuroscience. 1998; 18:4825–4832. [PubMed: 9634548]

Sabri O, Becker GA, Meyer PM, Hesse S, Wilke S, Graef S, … Brust P. First-in-human PET quantification study of cerebral a4b2* nicotinic acetylcholine receptors using the novel specific radio-ligand (-)-[18F]flubatine. NeuroImage. 2015; 118:199–208. [PubMed: 26037057]

Savitz JB, Bonne O, Nugent AC, Vythilingam M, Bogers W, Charney DS, Dreverts WC. Habenula volume in post-traumatic stress disorder measured with high-resolution MRI. Biology of Mood & Anxiety Disorders. 2011; 1:7. [PubMed: 22738208]

Schweinhardt P, Fransson P, Olson L, Spenger C, Andersson JL. A template for spatial normalisation of MR images of the rat brain. Journal of Neuroscience Methods. 2003; 129:105–113. [PubMed: 14511814]

Semsei I. On the nature of aging. Mechanisms of Ageing and Development. 2000; 117:93–108. [PubMed: 10958926]

St John PA. Cellular trafficking of nicotinic acetylcholine receptors. Acta Pharmacologica Sinica. 2009; 30:656–662. [PubMed: 19498414]

Sultzer DL, Melrose RJ, Riskin-Jones H, Narvaez TA, Veltz J, Ando TK, … Mandelkern MA. Cholinergic receptor binding in Alzheimer disease and healthy aging: Assesment in vivo with positron emission tomography imaging. American Journal of Geriatric Psychiatry. 2017; 25:342–353. [PubMed: 28162919]

Thomas B, Eyssen M, Peeters R, Molenaers G, Van Hecke P, De Cock P, Sunaert S. Quantitative diffusion tensor imaging in cerebral palsy due to periventricular white matter injury. Brain. 2005; 128:2562–2577. [PubMed: 16049045]

Tohgi H, Utsugisawa K, Yoshimura M, Nagane Y, Mihara M. Age-related changes in D1 and D2 receptor mRNA expression in postmortem human putamen with and without multiple small infarcts. Neuroscience Letters. 1998; 243:37–40. [PubMed: 9535107]

Tribollet E, Bertrand D, Marguerat A, Raggenbass M. Comparative distribution of nicotinic receptor subtypes during development, adulthood and aging: An autoradiographic study in the rat brain. Neuroscience. 2004; 12:405–420.

Tweed JO, Hsia SH, Lufty K, Friedman TC. The endocrine effects of nicotine and cigarette smoke. Trends in Endocrinology and Metabolism. 2012; 23:334–342. [PubMed: 22561025]

Vaupel DB, Tella SR, Huso DL, Wagner VO 3rd, Mukhin AG, Chefer SI, … Kimes AS. Pharmacological and toxicological evaluation of 2-fluoro-3-(2(S)-azetidinylmethoxy)pyridine (2-F-A-85380), a ligand for imaging cerebral nicotinic acetylcholine receptors with positron emission tomography. Journal of Pharmacological Experimental Therapeutics. 2005; 312:355–365.

Volkow ND, Gur RC, Wang GJ, Fowler JS, Moberg PJ, Ding YS, … Logan G. Association between decline in brain dopamine activity with age and cognitive and motor impairment in healthy individuals. American Journal of Psychiatry. 1998; 155:344–349. [PubMed: 9501743]

Wada E, Wada K, Boulter J, Deneris E, Heineman S, Patrick J, Swanson LW. Distribution of alpha2, alpha3, alpha4, and beta2 neuronal nicotinic receptor subunit mRNAs in the central nervous system: A hybridization histochemical study in the rat. Journal of Comparative Neurology. 1989; 284:314–335. [PubMed: 2754038]

Whiteaker P, Wilking JA, Brown RWB, Brennan RJ, Collins AC, Lindstrom JM, Boulter J. Pharmacological and immunochemical characterization of a2* nicotinic acetycholine receptors (nAChRs) in mouse brain. Acta Pharmacologica Sinica. 2009; 30:795–804. [PubMed: 19498420]

Xiu X, Puskar NL, Shanata JAP, Lester HA, Dougherty DA. Nicotine binding to brain receptors requires a strong cation-p interaction. Nature. 2009; 458:534–537. [PubMed: 19252481]

Xiao Y, Kellar KJ. The comparative pharmacology and up-regulation of rat neuronal nicotinic receptor subtype binding sites stably expressed in transfected mammalian cells. Journal of Pharmacological and Experimental Therapeutics. 2004; 310:98–107.

Xu J, Azizian A, Monterosso J, Domier CP, Brody AL, Fong TW, London ED. Gender effects on mood and cigarette craving during early abstinence and resumption of smoking. Nicotine Tobacco Research. 2008; 10:1653–1661. [PubMed: 18988078]

Yu D, Yuan K, Zhang B, Liu J, Dong M, Jin C, Luo L, Zhai J, Zhao L, Zhao Y, Gu Y, Xue T, Liu X, Lu X, Qin W, Tian J. White matter integrity in young smokers: a tract-based statistics study. Addiction Biology. 2016; 21:679–687. [PubMed: 25752453]

Zanchi D, Brody A, Borgwardt S, Haller S. Sex effects on smoking cue perception in non-smokers, smokers, and ex-smokers: A pilot study. Frontiers Psychiatry. 2016; 7:187.

Zemkova H, Kucka M, Bjelobaba I, Tomic M, Stojilkovic SS. Multiple cholinergic signaling pathways in pituitary gonadotrophs. Endocrinology. 2013; 154:421–433. [PubMed: 23161872]

Zoli M, Pistillo F, Gotti C. Diversity of native nicotinic receptor subtypes in mammalian brain. Neuropharmacology. 2015; 96(Pt B):302–311. [PubMed: 25460185]

Zuo Y, Garg PK, Nazih R, Garg S, Rose JE, Murugesan T, Mukhin AG. A programmable smoke delivery device for PET imaging with cigarettes containing 11C-nicotine. Journal of Neurscience Methods. 2017; 283:55–61.

Zuo Y, Mukhin AG, Garg S, Nazih R, Behm FM, Garg PK, Rose JE. Sex-specific effects of cigarette mentholation on brain nicotine accumulation and smoking behavior. Neuropsychopharmacology. 2015; 40:884–892. [PubMed: 25267342]
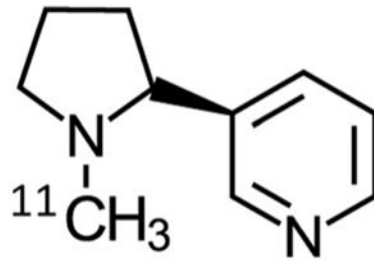
a. [^{11}C]Nicotine
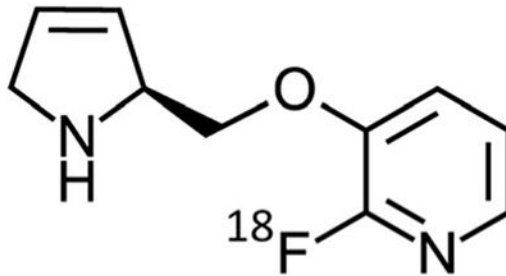
b. [^{18}F]Nifene

FIGURE 1. Chemical structures
(a). Structure of [^{11}C]Nicotine. (b). Structure of [^{18}F]Nifene used in the studies
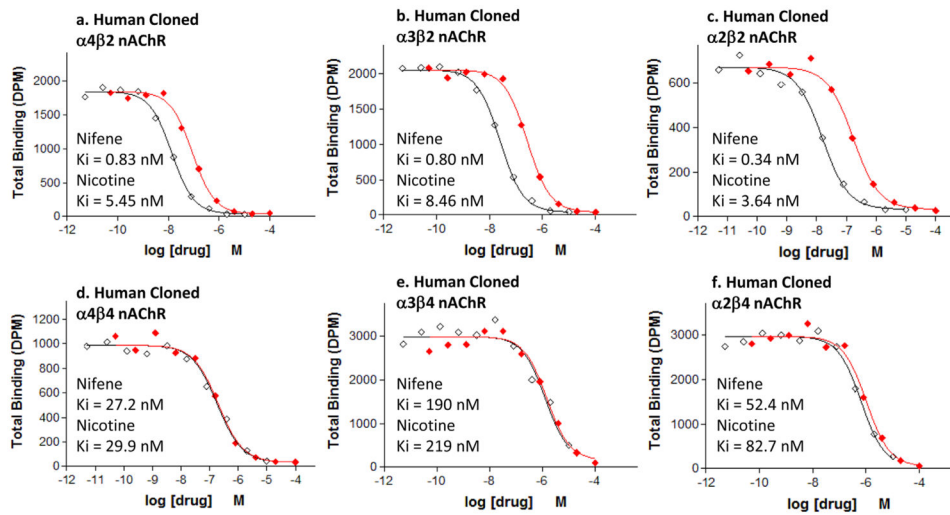
FIGURE 2. In vitro receptor binding profiles of Nifene (blue curves; PDSP Compound #38026) for human cloned receptors

(a). nAChR α4β2 (Ki =0.83 nM). (b) nAChR α3β2 (Ki =0.80 nM). (c) nAChR α2β2 (Ki =0.34 nM). (d). nAChR α4β4 (Ki =27.2nM). (e). nAChR α3β4 (Ki =190 nM). (f). nAChR α2b4 (Ki =52.4 nM). Affinities of reference compound nicotine (red curves) were found to be weaker for all these receptor subtypes. [Color figure can be viewed at wileyonlinelibrary.com]
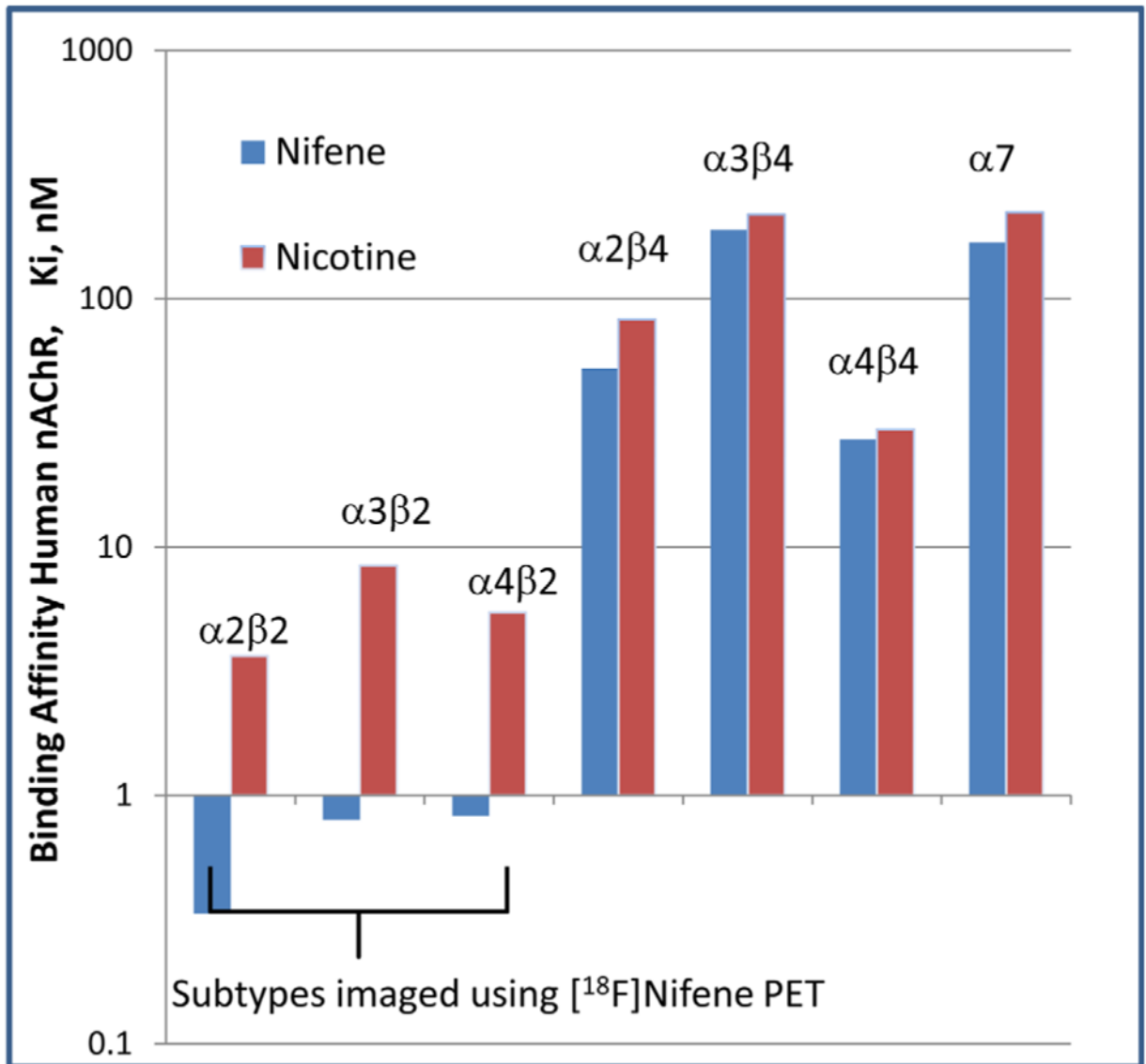
FIGURE 3. Comparison of nicotine and Nifene at different nicotinic receptor subtypes
Subnanomolar affinity of Nifene for α2β2, α3β2 and α4β2 indicates potential in vivo imaging of the three subtypes by ^{18}F-Nifene. [Color figure can be viewed at wileyonlinelibrary.com]
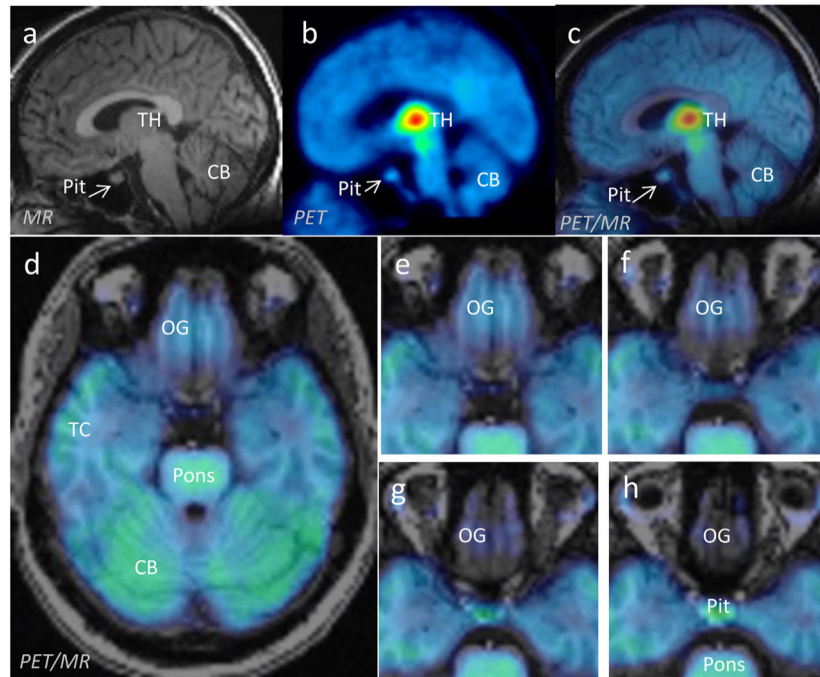
FIGURE 4. Pituitary and Olfactory Human [18F]Nifene PET

(a–c). Sagittal brain slices (a: MR; b: PET and c: PET/MR) showing [18F]Nifene (DVR) in the pituitary gland (Pit). (d). Coregistered PET/MRI of transaxial brain slice showing olfactory gyri (OG), temporal cortex (TC), pons and cerebellum (CB). (e–h). Sequential close up (x2) slices of OG showing distinct [18F]Nifene binding. [Color figure can be viewed at wileyonlinelibrary.com] of 1.75 ± 0.09 in females versus 1.60 ± 0.08 in males, suggesting 9% higher in females compared to males (p-value of 0.045). Other regions of the brain showed minor differences, but overall females had higher DVR values.
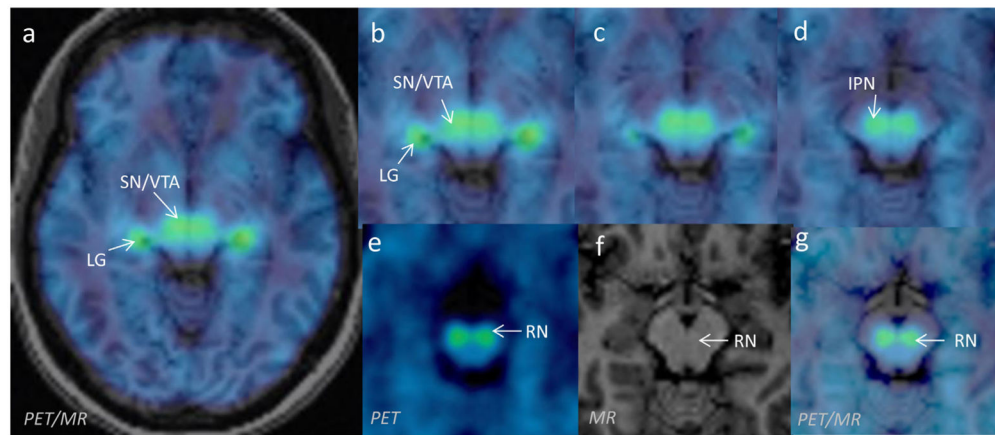
FIGURE 5. IPN and RN α2β2 Regions Human [^{18}F]Nifene PET
(a). Transaxial brain slice of [^{18}F]Nifene (DVR) in the human midbrain region showing substantia nigra/ventral tegmental areas (SN/VTA). Also present in this brain slice is lateral geniculate (LG). (b–g). Close up (x2) view of the midbrain showing possible bilateral interpeduncular nucleus (IPN) in (d) and red nucleus (RN) seen in PET (e), MR (f) and coregistered PET/MR (g). [Color figure can be viewed at wileyonlinelibrary.com]
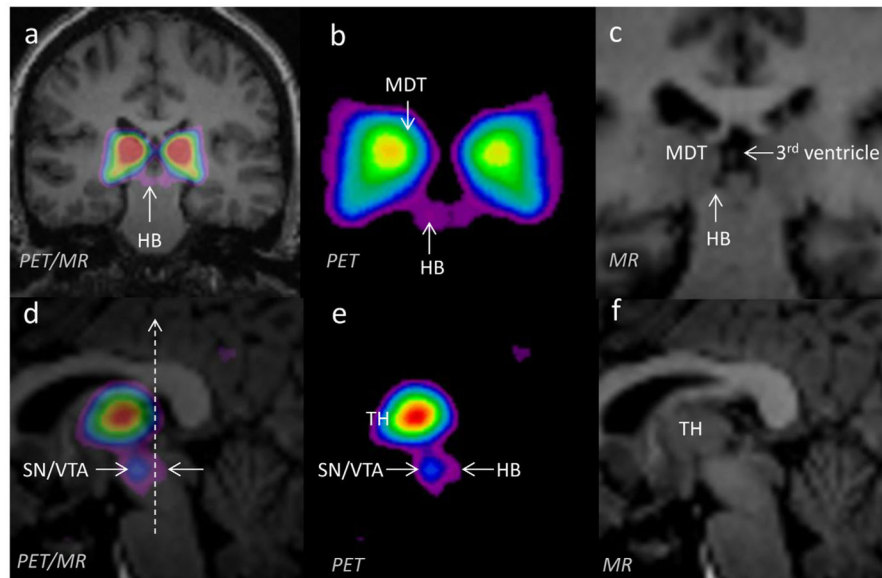
FIGURE 6. Habenula α3β2 Regions Human [^{18}F]Nifene PET
(a, d). Coronal and sagittal PET/MR brain slice of [^{18}F]Nifene (DVR) through the habenula (HB). (b, e). Close-up of PET images of (a, d) showing HB and medial dorsal thalamus (MDT) and HB posterior to substantia nigra/ventral tegmental area (SN/VTA). (c, f). Close-up of MR images of (a, d) showing HB by the 3rd ventricle and corresponding sagittal brain slice. [Color figure can be viewed at wileyonlinelibrary.com]
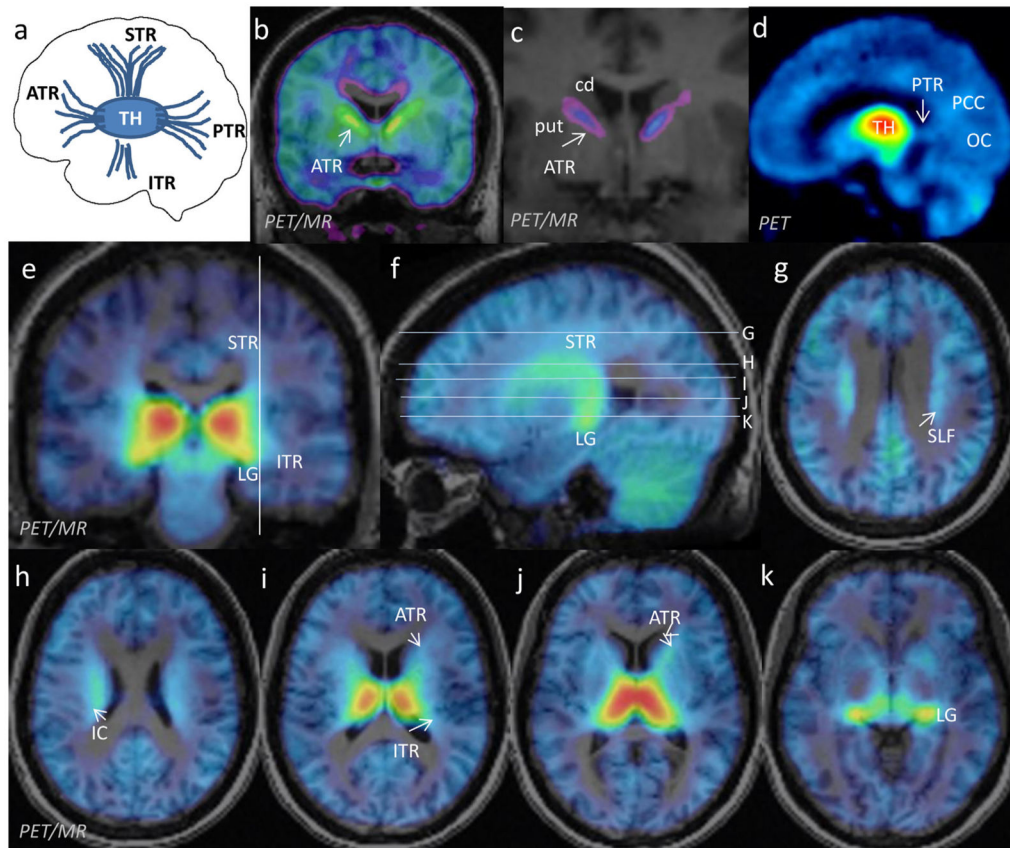
FIGURE 7. Thalamic Radiations (TR) using [^{18}F]Nifene PET

(a). Schematic showing the four thalamic radiations of [^{18}F]Nifene (DVR) (ATR: anterior; STR: superior; ITR: inferior; PTR: posterior thalamic radiations). (b). PET/MR coronal slice of ATR emerging from the thalamus and passing through internal capsule white matter between the caudate and putamen. (c). Close-up view of (b) showing ATR bundle passing between caudate (cd) and putamen (put). (d). Sagittal PET slice showing PTR extending from the thalamus (TH) to the posterior cingulate (PCC) and occipital cortex (OC). (e). Coronal PET/MR slice showing STR to the parietal cortex (PC) and ITR to the temporal cortex (TC) and auditory cortex (AC). The vertical line in proximity to the lateral geniculate (LG) was used to show the sagittal slice in (f). (f). PET/MR sagittal slice showing STR bundles extending up to the PC via the white matter. Five horizontal slices (g–k) are shown. (g). Superior longitudinal fasciculus (SLF) white matter tract showing [^{18}F]Nifene binding. (h). Thalamic radiation from the internal capsule (IC) showing [^{18}F]Nifene binding. (i). [^{18}F]Nifene ATR to the frontal cortex and ITR to the temporal cortex. (j). ATR via IC to the frontal cortex, corresponding to coronal slices (b) and (c). (K). Lateral geniculate (LG) and cortical structures labeled with [^{18}F]Nifene. [Color figure can be viewed at wileyonlinelibrary.com]
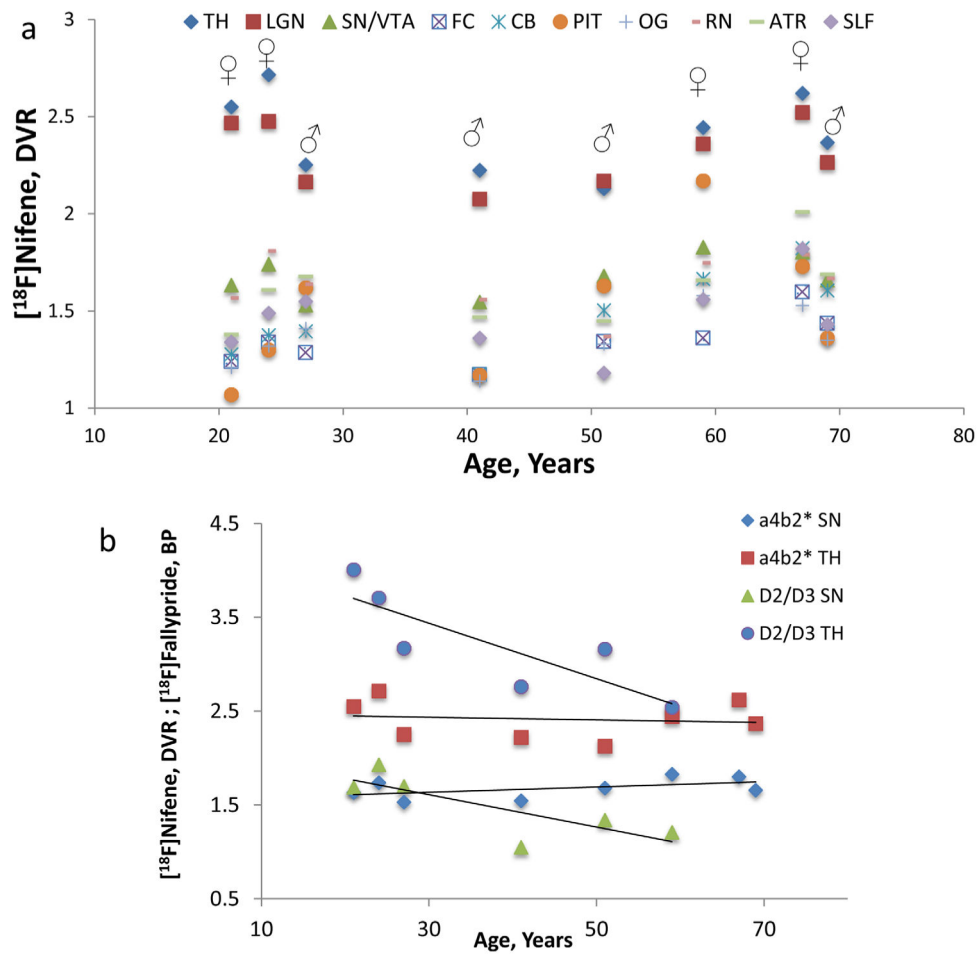
FIGURE 8. Aging Effects in Human [^{18}F]Nifene PET

(a). Plot of [^{18}F]Nifene PET DVR versus age in male and female subjects (TH: thalamus; LGN: lateral geniculate; SN/VTA: substantia nigra/ventral tegmental area; FC: frontal cortex; CB: cerebellum). (b). Comparison of human aging effects in two receptor systems-α4β2* nAChR ([^{18}F]Nifene) and dopamine D2/D3 receptors ([^{18}F]Fallypride) in two brain regions, thalamus (TH) and substantia nigra (SN). [Color figure can be viewed at wileyonlinelibrary.com]
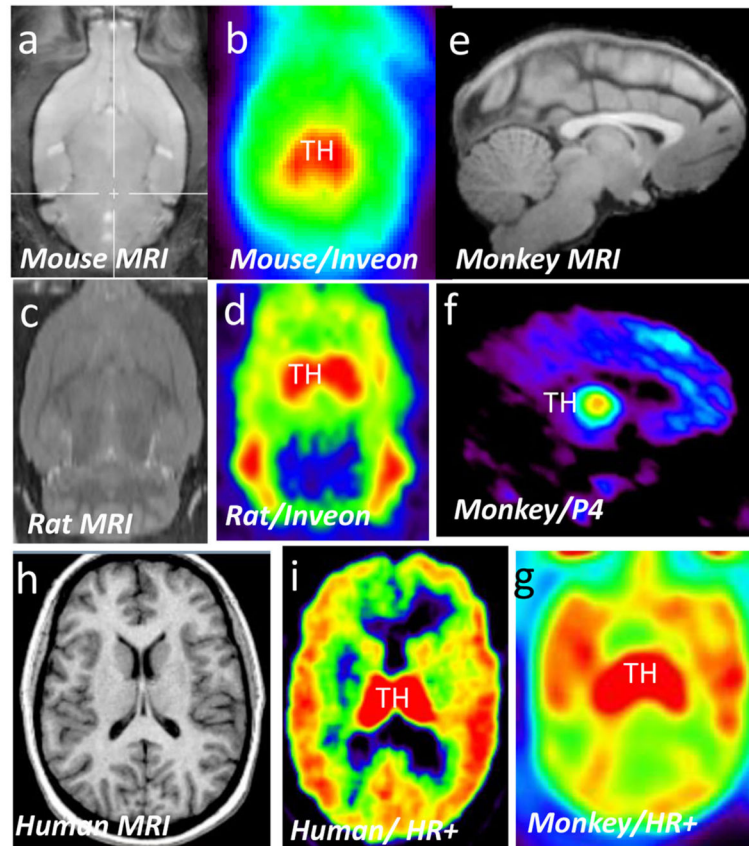
FIGURE 9. PET images across species of [^{18}F]Nifene
(a). Mouse brain slice from coregistered MRI template. (b). Mouse brain PET slice corresponding to MRI slice in A. (c). Rat brain slice from coregistered MRI template. (d). Rat brain PET slice corresponding to MRI slice in C. (e). Monkey brain slice from coregistered MRI template. (f) Monkey brain PET slice on P4 Focus scanner corresponding to MRI slice in E. (g). Monkey brain PET slice on ECAT EXACT HR+ scanner. (h). MRI brain slice of human subject shown in I. (i). Human brain PET slice of subject shown in Fig-9h on ECAT EXACT HR+ scanner. [Color figure can be viewed at wileyonlinelibrary.com]

TABLE 1

Binding affinity and selectivity for Nifene and nicotine at human nAChRs[a]

Tracer	α4β2	α3β2	α2β2	α4β4	α3β4	α2β4	α7
Nifene, Ki nM	0.83[b]	0.80[b]	0.34[b]	27.2[b]	190[b]	52.4[b]	169[e]
% human α4β2 Selectivity[f,g]	1.07[c], 0.50[d] 100	104	244	3.05	0.44	1.58	0.63[h]
Nicotine, Ki nM	5.45[b]	8.46[b]	3.64[b]	29.9[b]	219[b]	82.7[b]	223[e]
% human α4β2 Selectivity[f,g]	6.93[c], 1.68[d] 100	64.4	150	18.2	2.49	6.59	3.11[h]

[a] Human cloned receptor affinities obtained from pdsp.unc.edu.

[b] Assays using human cloned receptors using ^{3}H-epibatidine.

[c] Rat brain cortex labeled with ^{3}H-epibatidine (pdsp.unc.edu).

[d] Rat brain homogenates labeled with ^{3}H-cytisine (Pichika et al., 2006).

[e] Rat cloned receptors labeled with ^{125}I-α-bungarotoxin (pdsp.unc.edu).

[f] Percent selectivity for α4β2 receptor =[α4β2 affinity/other receptor affinity]×100.

[g] Calculated assuming human receptor affinities of 0.83 nM for Nifene and 5.45 nM for Nicotine for the α4β2 receptor.

[h] Calculated assuming rat affinities of 1.07 nM for Nifene and 6.93 nM for Nicotine for the α4β2 receptor.

TABLE 2

Functional assay of Nifene[a]

Nifene	α4β2 nAChR		α3β4 nAChR	
	As Agonist[b]	As Antagonist[c]	As Agonist[b]	As Antagonist[c]
1 μM	–	18%	–	9%
10 μM	–	21%	–	16%
100 μM	14%	56%	35%	59%

[a] Nifene was tested for its agonist and antagonist effects on Rb^+ efflux from YXα3β4H1 and YXα4β2H1 cells that stably express functional human α3β4 and human α4β2 nAChR subtypes (pdsp.unc.edu).

[b] Determined by measuring stimulated $^{86}Rb^+$ efflux in presence of Nifene. Net stimulated $^{86}Rb+$ efflux by 100 μM nicotine as 100%. Data are mean % of stimulation of 4 determinations.

[c] The antagonist effect was determined by measuring inhibition of 100 μM nicotine-stimulated $^{86}Rb^+$ efflux by 3 concentrations of Nifene. Net stimulated $^{86}Rb+$ efflux by 100 μM nicotine as 0% inhibition. Data are mean % of inhibition of 4 determinations.

TABLE 3

18F-Nifene human gender effects

	Age	Brain Regions, DVR values									
		Thalamus	LG	SN/VTA	Frontal cortex	CB	Pit	OG	Red Nucleus	ATR	SLF
Females	21	2.55	2.47	1.63	1.24	1.28	1.07	1.21	1.57	1.38	1.34
	24	2.72	2.48	1.74	1.34	1.38	1.30	1.32	1.81	1.61	1.49
	59	2.44	2.36	1.83	1.36	1.67	2.17	1.58	1.75	1.66	1.56
	67	2.62	2.52	1.80	1.60	1.82	1.73	1.53	1.79	2.01	1.82
Avg±SD		2.58 ± 0.11	2.46 ± 0.07	1.75 ± 0.09	1.38 ± 0.15	1.54 ± 0.25	1.57 ± 0.49	1.41 ± 0.17	1.73 ± 0.11	1.67 ± 0.26	1.55 ± 0.20
Males	27	2.25	2.17	1.53	1.29	1.40	1.62	1.41	1.64	1.68	1.55
	41	2.22	2.08	1.55	1.17	1.18	1.17	1.14	1.56	1.47	1.36
	51	2.13	2.17	1.68	1.34	1.50	1.63	1.33	1.37	1.45	1.18
	69	2.37	2.26	1.66	1.44	1.61	1.36	1.35	1.67	1.69	1.43
Avg±SD		2.24 ± 0.10	2.17 ± 0.08	1.60 ± 0.08	1.31 ± 0.11	1.42 ± 0.18	1.45 ± 0.22	1.31 ± 0.12	1.56 ± 0.13	1.58 ± 0.13	1.38 ± 0.15
♀ vs ♂ [a]p-value		0.004*	0.001*	0.045*	0.45	0.49	0.67	0.37	0.10	0.56	0.23

LG: Lateral geniculate; SN/VTA: Substantia nigra/Ventral tegmental area; CB: cerebellum; Pit: Pituitary gland; OG: Olfactory gyri; ATR: Anterior thalamic radiation; SLF: Superior longitudinal fasciculus.

[a] p Values computed for female-male difference using two-tailed, two-sample unequal variance.